CMS TN/95-128

First Evaluation of the Curvature Sampling Pattern Recognition Algorithm in context of the CMS Inner Tracker

S.Banerjee, F.Bruyant
CERN/ECP

S.Piperov
Sofia University and INRNE - Sofia

24 November 1995

Abstract

The *Curvature Sampling* pattern recognition algorithm performs a global track finding, returning the azimuthal angle φ_0 and the transverse momentum p_T of all tracks coming from the interaction region with p_T over a given cut value. It is based on a histograming technique, made fast through the use of a (reasonable) number of precomputed quantities.

Preliminary results in the context of the CMS Inner Tracker are presented. They look rather promising.

1 Introduction

The basic idea of the *Curvature Sampling* algorithm and the successive pattern recognition steps suggested to extract the 3D track parameters have been presented in an earlier note [1]. The first step is to find an approximation of the track parameters in xy projection. This is the only one discussed in this note. Let us briefly recall here what it consists of.

It is assumed that the initial data consist of measurements in a cylindrical coordinate system (polar coordinates r and φ, z coordinate along the direction of the magnetic field) [1].

Given the geometry of the magnet the charged particle trajectories are helicoidal [2]. For any particle coming from a primary interaction the xy projection of the trajectory is a circle, parameterized as follows:

$$f_i(R_{ref}) \;=\; \varphi_i - \arcsin(c * r_i/2) + 2 * \arcsin(c * R_{ref}/2)$$

where r_i, φ_i are the polar coordinates of the ith measurement,

c, the (signed) curvature,

$f_i(R_{ref})$, the azimuthal angle of the trajectory at $r = R_{ref}$.

Every measurement point is considered as potentially belonging to (at least) one charged particle trajectory. For any point the assumption is therefore made that it belongs to either one of a number of fictitious trajectories obtained by sampling the curvature between $-c_{\max}$ and $c_{\max}$ by steps of Δc. For all points belonging to a real trajectory the values of f computed with the closest sampled curvature are expected to be the same (see Fig.1). This should generate a peak in the scatter plot f versus c.

A priori, three values of R_{ref} can be used:

near the origin vertex (option BEG, $R_{ref} = 0$),

the maximum radial dimension $r_{\max}$ of the tracker (option END, $R_{ref} = 120$ cm),

half way through (option MID, $R_{ref} = 60$ cm).

2 Implementation of the algorithm in CMSIM100

The event data are produced using a preliminary version of CMSIM100 [2], the Monte-Carlo simulation program for the CMS detector.

Except for a few actions performed directly within PAW [3], the code developed for this study is inserted into CMSIM100, using the so-called User Hooks, a set of subroutines for user intervention at different stages of the execution (reading data cards, booking histograms, taking action at every tracking step, filling histograms and doing analysis).

[1] In the current design of the tracker the radial information provided by some of the chamber planes is too unprecise and requires special treatment, as discussed in 3.5

[2] At least for particles with moderate energy loss

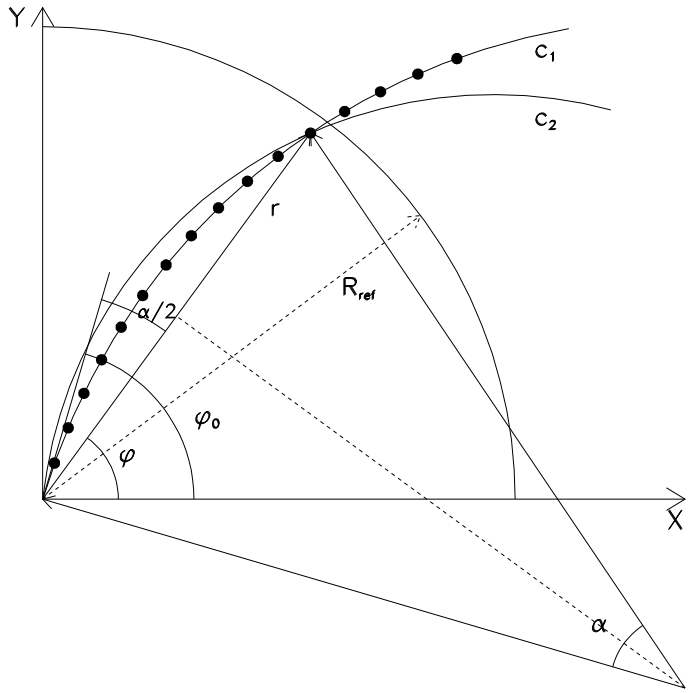

Figure 1: Curvature sampling

Provisionally, the polar coordinates of the track measurements are computed at the entrance of each sensitive detector element. This seems an over-simplification of the problem but the algorithm turns out to be quite tolerant, as one can see in 3.3, and the approximation should not affect the conclusions of this preliminary study.

3 Single track studies

3.1 Bin sizes in c and f

The peak structure in the scatter plot f versus c is expected to be strongly dependent on the (correlated) bin sizes in c and f. Assuming a realistic number of bins, at most 50 for each curvature sign, the bin size in c depends on the p_T cut. For instance, for $p_T > 1$ GeV/c the bin size Δc should not be less than 0.0002 cm^{-1}. The variation δf corresponding to a curvature variation δc (equal to half the bin size Δc) is

$$\delta f = (R_{ref} - r/2) * \delta c$$

Assuming $\Delta c = 0.0002$ cm^{-1} one obtains the following results for the three options BEG, MID and END.

BEG: $\delta f = -0.06, -0.34, -0.67$ (for $r = 10, 60, 120$ respectively)

MID: $\delta f = 0.62, 0.34, 0.$

END: $\delta f = 1.28, 1.01, 0.67$

The smallest variation in f is obtained for the option MID. This option has also its largest acceptance for the smallest r values, favouring the situation where the tracks have a non negligible impact parameter with respect to their assumed origin ($x = 0.$, $y = 0.$). Because of the arbitrariness in the choice of the origin on the f axis, it seems reasonable to choose a bin size Δf equal to half δf, which guarantees that all measurements belonging to the trajectory will fall within three neighbouring bins. As mentioned later, other arguments should be considered, in particular the rejection of points not belonging to the track.

3.2 Single track results

The behaviour of individual tracks is illustrated in Fig. 2, 3, 4 and 5. The scatter plots for a high energy μ^+ ($p_T = 41.4$ GeV/c, $\phi_0 = 180°$ and $\eta = 1.57$) are shown in Fig. 2a, 2b, 2c, for the options BEG, MID and END respectively. Assuming a magnetic field of 4 Tesla, the value of the momentum corresponds exactly to the value of the sampled curvature (the most favourable case, the centre of the bin). The structure of the peaks is exactly as expected. In Fig. 3a, 3b, 3c, the value of the momentum (30 GeV/c) corresponds to the worse situation, with the curvature equal to the value at one edge of the bin. Here again the structure of the peaks behaves as expected. Fig 4 and 5 show the same plots for particles with $\eta = 0$ and p_T of 1.62 GeV/c and 1.58 GeV/c respectively (corresponding to the centre and the edge of the sampled curvatures). In Fig 5 the combined effect of energy loss and multiple scattering is observable, still tolerable. It is worth noting that, in all scatter plots, the details of the peak structure allow to estimate f and c with more precision than what could be deduced directly from the indices of the most populated bin.

3.3 Randomizing the measurement points

In order to test how the algorithm would work with data more realistic than the precise polar coordinates used for this study, the latter are randomized on circles of radius equal to 200 μm (for the silicon detectors) and 500 μm (for the gas chambers) centered at the original measurements. As shown on Fig 6, the peaks are not much altered. This gives some confidence in the robustness of the algorithm.

3.4 Impact parameter with respect to assumed particle origin

It is important to check the ability of the algorithm to find particle trajectories with not too small impact parameters with respect to the assumed origin.

Transverse shifts up to the order of a few millimeters do not affect the peaks significantly, as shown in Fig 7. Of course the values of f and c at the peak are biased, but a fit of φ_0, c and

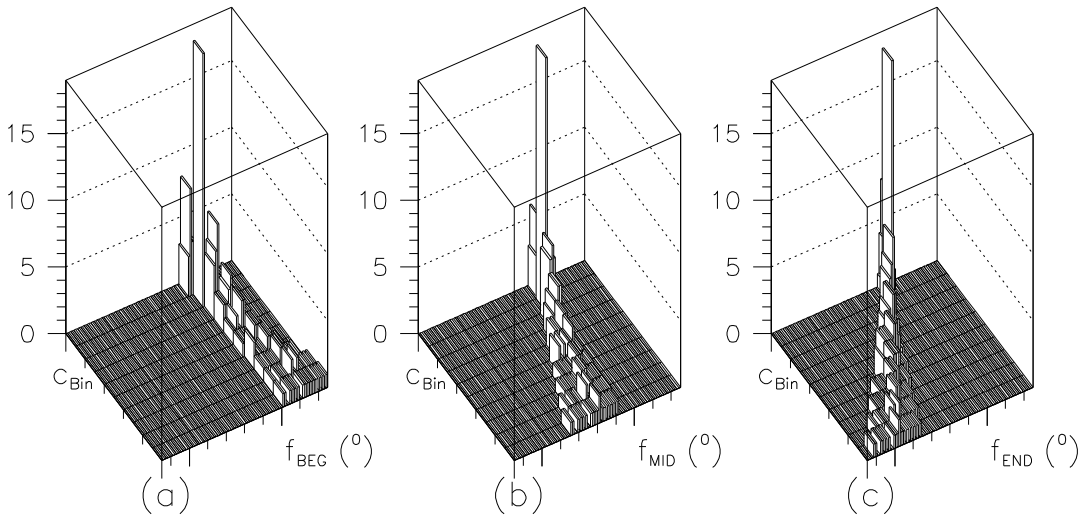

Figure 2: f versus c plot for μ^+ with $p_T = 41.4$ GeV/c, $\phi_0 = 180°$ amd $\eta = 1.57$

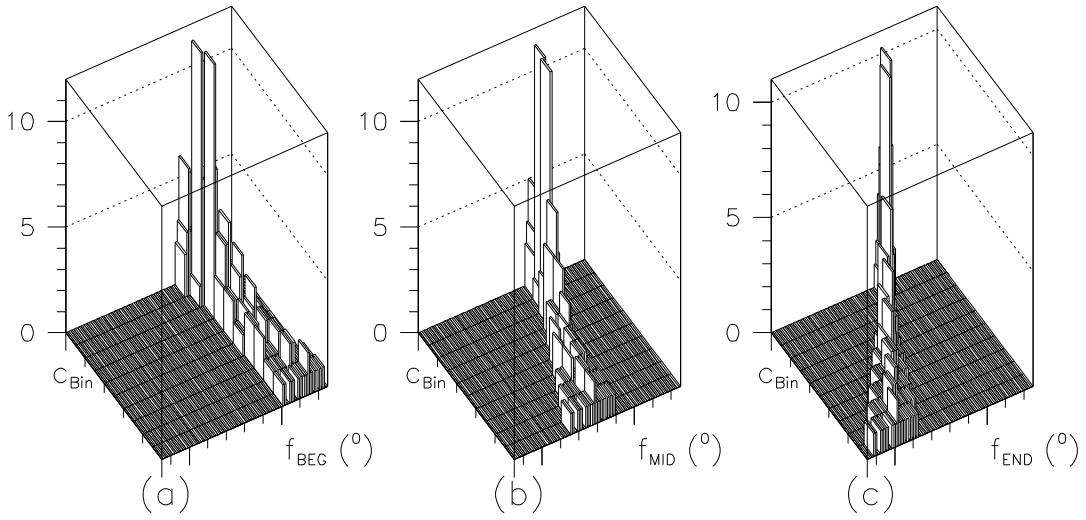

Figure 3: f versus c plot for μ^+ with $p_T = 30.0$ GeV/c, $\phi_0 = 180°$ amd $\eta = 1.57$

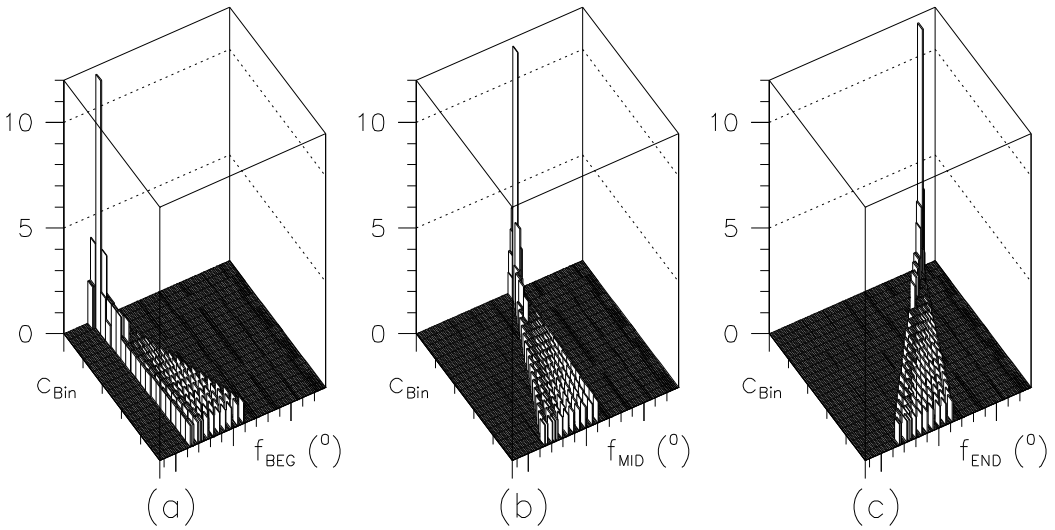

Figure 4: f versus c plot for μ^+ with $p_T = 1.62$ GeV/c, $\phi_0 = 180°$ amd $\eta = 0$

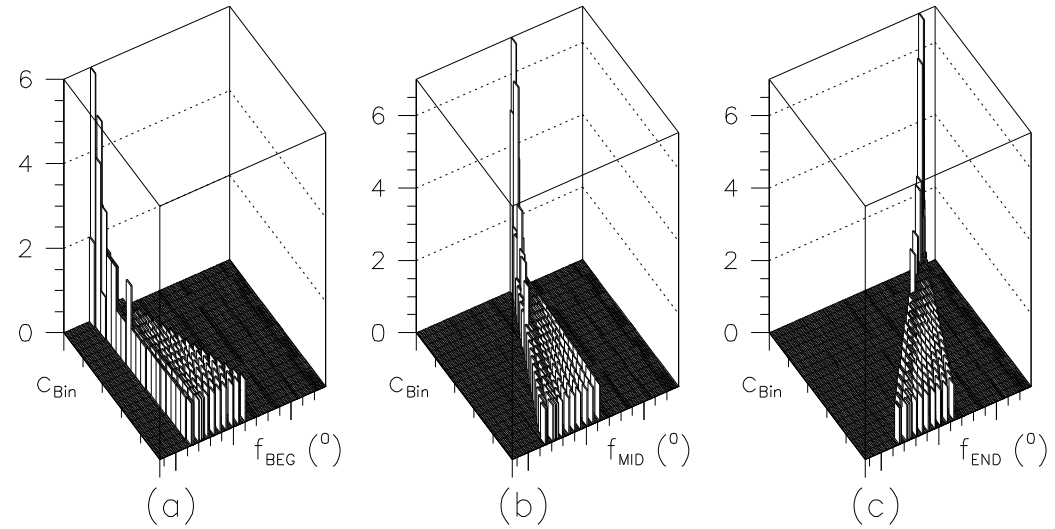

Figure 5: f versus c plot for μ^+ with $p_T = 1.58$ GeV/c, $\phi_0 = 180°$ amd $\eta = 0$

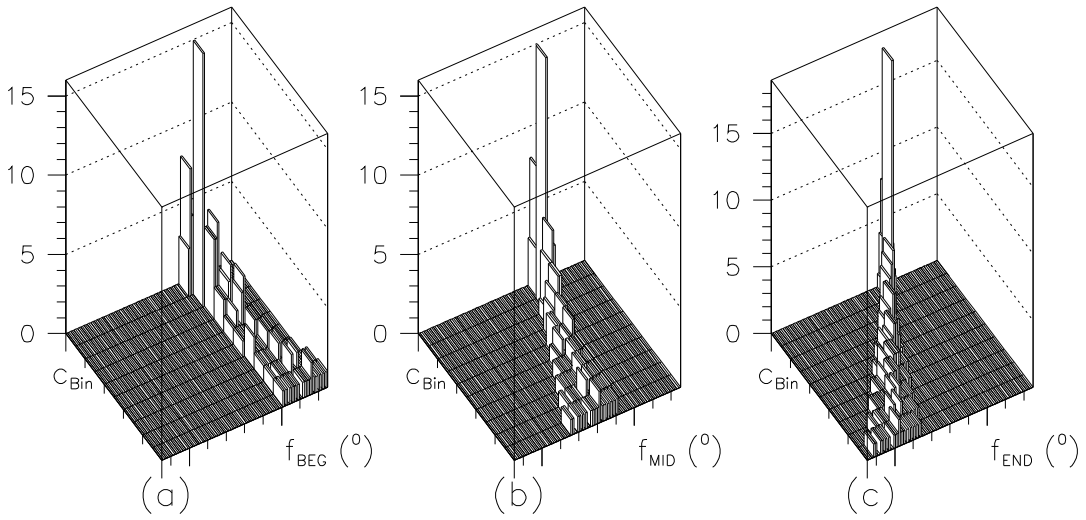

Figure 6: f versus c plot for μ^+ with $p_T = 41.4$ GeV/c, $\phi_0 = 180°$ amd $\eta = 1.57$. The hits in the silicon detectors are randomized with an error of 200 μm and those in MSGC with an error of 500 μm.

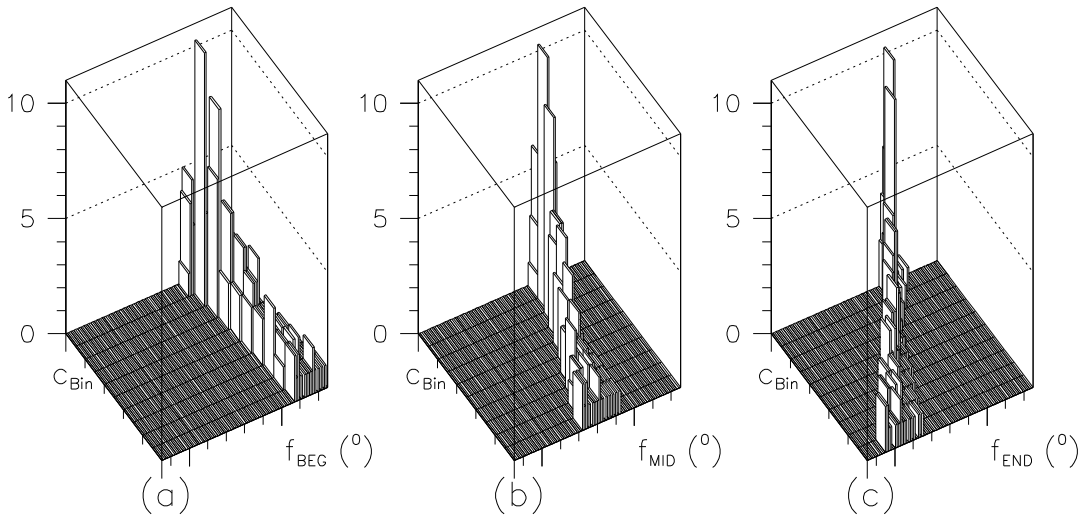

Figure 7: f versus c plot for μ^+ with $p_T = 41.4$ GeV/c, $\phi_0 = 180°$ and $\eta = 1.57$. The vertex has a shift of 0.28 cm along in the transverse direction.

the impact parameter d, as described in [4], would provide the correct values. Let us recall here the proposed least square fit, suitable even for high curvatures (as long as the approximation $\sin(\alpha) = \alpha - \alpha^3/3!$ stays valid):

$$\varphi = \varphi_0 + \alpha * r + \beta * r^3 + d/r$$

with $\alpha = c/2$ and $\beta = -\alpha^3/6$. [3]

3.5 Fake measurements in the end-cap strips

For the end-cap cells with poor radial precision, it is suggested to simulate cell divisions, thus generating temporary artificial measurements to enhance the peaks, making possible the identification of the trajectories. In practice, the treatment could consist of predicting bands in r, making use of an independent stereo information.

Tests of the idea applied to single particles show that the peaks are indeed enhanced and that the efficiency of the algorithm could be preserved.

4 Multi-track context.

4.1 Bin sizes in c and f

For pile-up events with large multiplicities and an impressive density of measurements, the bin sizes have to be determined in order to be as selective as possible, taking into account the following constraints:

- a not too large number of curvature samplings, the number of entries in the scatter plot being equal to the number of measurements times the number of samplings,
- the need to also capture tracks with not too small impact parameters.

Ultimately, the intrinsic resolution characteristics of the various types of detectors may usefully be considered.

In practice, there are two ways to proceed, either to enlarge the bins and to let the fit algorithm the responsibility of removing the spurious measurements (after trivial elimination of measurements with incompatible z values, as suggested in [1]), or to tune the bin sizes tightly, discarding eventually in a first pass the chambers too close to the interaction region, then to redo a scatter plot only for the measurements within a narrow 3D road, with impact parameter corrections if necessary and with a few curvature samplings centered around the value of the curvature obtained from the first pass.

[3] In ref [4], β is given equal to $-\alpha^3/3$.

4.2 Scatter plot edge effects

In order to eliminate the risk of missing any peaks close to the histogram edges in f (0° or 360°), the histograms are booked with a few more bins below 0° and over 360°) and the entries in the overlap region are duplicated, once at the original position and once at the 'mirror' position.

Of course, this improves only the *visual* identification of the peaks.

4.3 A PYTHIA event

To assess the performance of the algorithm in a multi-track context, PYTHIA events have been generated, tracked through the detector and analyzed. So far, no powerful peak finding techniques have been used. For every event, the list of all tracks with p_T over the given p_T cut in the domain of acceptance of the detector is printed, as well as the information concerning the hits and the tracks to which they belong. From this one can deduce what the observed peaks consist of and estimate rather precisely whether the tracks could be reconstructed successfully.

At this stage, the discrete interaction processes have been switched off in order to understand what happens and to simplify the comparison between the tracks initially generated and the peaks found in the scatter plots. Both energy loss and multiple scattering have been activated. Secondary interactions generate tracks which have their origin anywhere and travel in all directions. It appears that some vicious configurations generate 'walls' at some values of f. These anomalies need to be investigated and understood before an efficient algorithm for peak identification can be adopted.

Fig 8 and Tables 1,2 show the behaviour of an event and display the details of the analysis. In Table 1, all particles with track index ITRA above 200 are decay products of short life particles decaying under control of the generator. Their impact parameters are of the order of a few millimeters. In Table 2, the quoted number of hits is the maximum of the sums of the number of hits in three adjacent bins in f including the bin where the peak was observed (namely, a bin with more than 6 hits). The quoted ambiguities concern the other peaks generated by the same particle in neighbouring bins in c and f and can easily be treated with a more realistic peak finding algorithm. All expected tracks are found. One ghost is also reconstructed, a mixture of background hits from many different tracks, which would not survive the tests in the third dimension z.

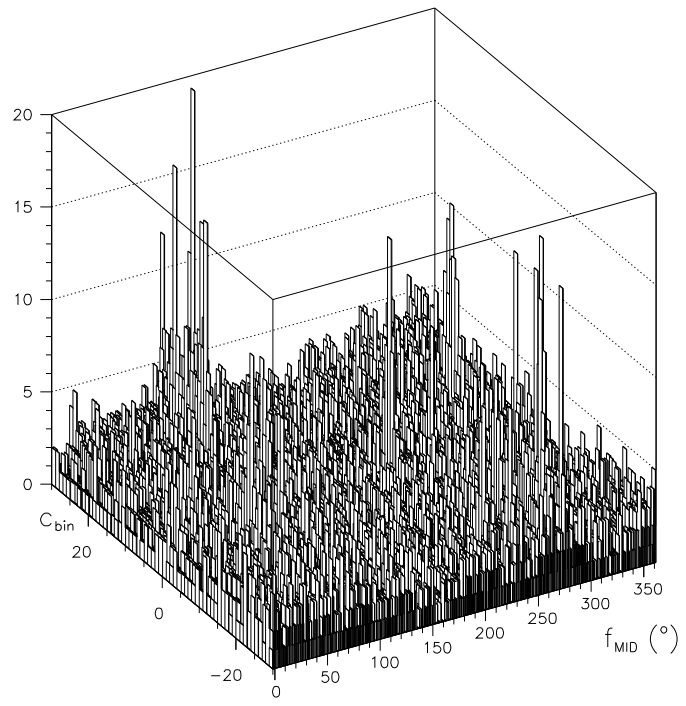

Figure 8: f versus c plot for a PYTHIA event at 14 TeV with a Higgs decaying to 4 muons

Table 1: List of all charged particles in event 1 with $p_T > 1$ GeV/c and $\eta < 2.5$

ITRA	Particle	p_T (GeV/c)	η	ϕ_0 (°)	ϕ_{mid} (°)	E (GeV)	# Hits
1	μ^-	40.78	2.41	29.1	30.2	229.74	10
2	μ^+	48.52	2.04	212.9	212.0	190.36	15
3	μ^-	31.52	1.76	96.2	97.6	94.02	13
4	μ^+	14.68	0.83	249.1	246.1	19.99	12
67	K^+	1.17	−1.83	252.4	213.5	3.79	13
69	K^-	3.59	−1.32	292.0	304.5	7.24	16
70	π^+	1.09	−1.35	273.9	232.0	2.26	18
86	π^-	1.03	−0.61	56.5	100.9	1.24	12
116	π^-	1.12	1.54	79.7	120.4	2.73	19
118	$\bar{p}$	1.45	2.27	76.4	107.7	7.17	13
122	K^+	2.11	1.76	82.6	61.3	6.30	13
123	$\bar{p}$	2.56	1.80	62.5	80.1	8.03	13
124	π^-	1.32	1.65	54.9	89.2	3.58	17
261	p	2.95	1.95	61.7	46.6	10.60	13
290	p	1.06	−1.04	320.0	277.0	1.94	15
309	π^+	1.51	1.45	319.0	289.1	3.38	19
318	π^+	1.15	1.66	306.4	266.8	3.14	17
319	π^-	2.25	1.66	297.3	317.2	6.12	17
320	π^+	1.30	1.52	308.1	273.2	3.11	19
322	π^+	1.49	2.39	275.5	245.2	8.24	10
352	K^+	2.30	1.92	308.9	289.3	8.03	13

Table 2: List of reconstructed tracks in event 1

ϕ Bin (°)	$p_T^{\min}$ (GeV/c)	$p_T^{\max}$ (GeV/c)	# Hits	# Ambiguities	ITRA
29.80	30.00	9999.00	11	0	1
46.40	3.00	3.33	17	2	261
61.20	2.14	2.31	15	1	122
79.60	2.50	2.72	18	3	123
88.80	1.30	1.43	22	0	124
96.80	30.00	9999.00	15	3	3
101.40	1.00	1.03	15	0	86
107.20	1.43	1.50	14	1	118
120.00	1.11	1.15	21	1	116
211.00	30.00	9999.00	12	2	2
214.00	1.15	1.20	14	1	67
232.00	1.11	1.15	20	1	70
245.40	1.50	1.58	12	1	322
245.60	15.00	30.00	15	2	4
267.60	1.15	1.20	18	1	318
274.00	1.36	1.43	20	2	320
277.00	1.07	1.11	17	1	290
289.60	1.58	1.67	20	2	309
289.80	2.50	2.73	15	2	352
299.00	30.00	9999.00	13	2	?
304.40	3.33	3.75	19	2	69
316.40	2.31	2.50	23	4	319

4.4 Some Suggestions

An easy way to improve the performance is achieved by dividing the tracker into several slightly overlapping rapidity regions, and filling separate scatter plots for each of them. Fig. 9a, 9b, 9c show the event of Fig. 8 with three regions up to rapidity $\mid \eta \mid = 1.76$.

It might also help to define, independently for each rapidity region, different bin sizes for the fast tracks (e.g. p_T over 5 GeV/c) and for the slower tracks, the latter being more affected by the energy loss, and to analyse the data with two scatter plots per region.

5 On-line applications

The gas chambers, because of their response time, provide signals integrated over several beam bunches. The fast silicon detectors (pixel and micro-strips) integrate only events belonging to the same bunch and could give valuable indications for on-line event triggering. Fig. 10 shows the event of Fig. 8 with only the pixel detector and the central part (barrel and a few end-cap disks) of the micro-strip silicon detectors.

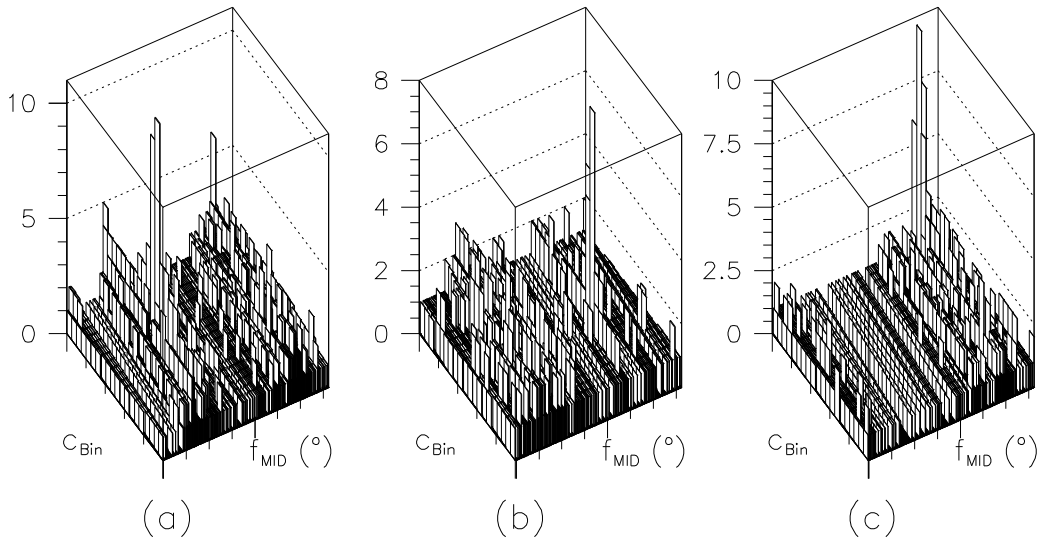

Figure 9: f versus c plot for the same event as in Fig. 8 divided into 3 slightly overlapping rapidity regions (a) $0.90 < \eta < 1.76$, (b) $-1.10 < \eta < 1.10$, (c) $-1.76 < \eta < -0.90$

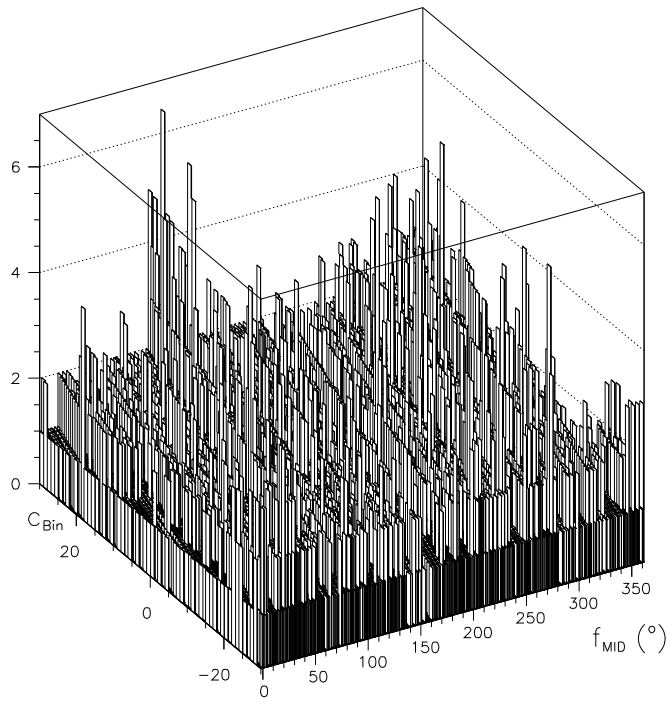

Figure 10: f versus c plot for the same event as in Fig. 8 using only the pixel detector and the central part of the silicon detectors

6 Conclusion

This preliminary study gives encouraging results. Further investigations are under way. A final evaluation for the CMS tracker requires more information on the performance of the chambers and on the configuration of the stereo planes.

References

[1] Proposed Pattern Recognition Algorithm for the CMS Inner Tracker, CMS-TN/95-125

[2] CMSIM100 Users' Guide, CMS detector simulation software group.

[3] PAW, The Complete Reference, CERN Program Library Long Writeup Q121

[4] European Spiral Reader Symposium, CERN Yellow Report 72-16